Sensor-Specific Error Statistics for SST in the Advanced Clear-Sky Processor for Oceans

B. PETRENKO

NOAA/STAR, College Park, and GST, Inc., Greenbelt, Maryland

A. IGNATOV

NOAA/STAR, College Park, Maryland

Y. KIHAI

NOAA/STAR, College Park, and GST, Inc., Greenbelt, Maryland

P. DASH

NOAA/STAR, College Park, Maryland, and Cooperative Institute for Research in the Atmosphere, Colorado State University, Fort Collins, Colorado

(Manuscript received 12 August 2015, in final form 4 December 2015)

ABSTRACT

The formulation of the sensor-specific error statistics (SSES) has been redesigned in the latest implementation of the NOAA Advanced Clear-Sky Processor for Oceans (ACSPO) to enable efficient use of SSES for assimilation of the ACSPO baseline regression SST (BSST) into level 4 (L4) analyses. The SSES algorithm employs segmentation of the SST domain in the space of regressors and derives the segmentation parameter from the statistics of regressors within the global dataset of matchups. For each segment, local regression coefficients and standard deviations (SDs) of BSST minus in situ SST are calculated from the corresponding subset of matchups. The local regression coefficients are used to generate an auxiliary product—piecewise regression (PWR) SST—and SSES biases are estimated as differences between BSST and PWR SST. Correction of SSES biases, which transforms BSST back into PWR SST, reduces the effects of residual cloud; variations in view zenith angle; and, during the daytime, diurnal surface warming. This results in significant reduction in the global SD of fitting in situ SST, making it comparable with SD for the Canadian Meteorological Centre (CMC) L4 SST. Unlike the foundation CMC SST (which is consistent with in situ SST at night but biased cold during the daytime), the PWR SST is consistent with in situ data during both day and night and thus may be viewed as an estimate of ''depth'' in situ SST. The PWR SST is expected to be a useful input into L4 SST analyses, especially for foundation SST products, such as the CMC L4.

1. Introduction

Sea surface temperature (SST; see the appendix for the list of acronyms used in this paper) is a key environmental variable that is routinely retrieved from satellite observations and is used in many applications. Several processing centers generate level 2 (L2) SST products from infrared satellite sensors data. To facilitate data exchange and use, the international Group for High Resolution SST (GHRSST) has established the GHRSST Data Specification revision 2.0 (GDS 2.0), format (the description is available at https://www.ghrsst.org/documents/q/category/ghrsst-data-processing-specification-gds/operational/). One of the GDS 2.0 requirements is that sensor-specific error statistics (SSES)—that is, estimates of SST bias and standard deviation (SD)—should be appended to each reported SST value. However, no specific guidance was provided on how the SSES should be calculated. As a result, different SSES definitions were implemented by EUMETSAT Satellite Application

Corresponding author address: Boris Petrenko, NOAA/STAR, 5830 University Research Court, College Park, MD 20740.
E-mail: boris.petrenko@noaa.gov

DOI: 10.1175/JTECH-D-15-0166.1

Facility on Ocean and Sea Ice (OSI-SAF; OSI-SAF 2009), NAVO (Cayula et al. 2004), NASA (Kilpatrick et al. 2015), and NOAA in the Advanced Clear-Sky Processor for Oceans (ACSPO) system (Petrenko and Ignatov 2014). Although the SSES is specifically intended to facilitate blending of different satellite L2 and L3 products and their assimilation into L4 analyses, the authors are not aware of any documented improvements in the data assimilation due to the use of any available SSES data. Consequently, the GHRSST-XV meeting in June 2014 has reviewed existing SSES practices and suggested revisiting those (GHRSST 2014, 197–199).

In this context, the ACSPO SSES has been redesigned with the explicit objective to achieve a positive effect on the L4 analyses. Typically, assimilation of satellite SSTs involves correction of biases in satellite SST with respect to in situ SST (or with respect to a reference satellite product) (e.g., Reynolds et al. 2002; Brasnett 2008; Donlon et al. 2012). Since many L4 products position themselves as "foundation" (defined at the depth below which no diurnal warming is present; Donlon et al. 2007) or "depth" (i.e., representative of in situ SSTs), our primary objective was achieving a measurable improvement in estimation of ACSPO SST biases with respect to in situ SST (and thus minimize the need for an empirical bias correction as an initial step of L4 processing). Another goal of the SSES redesign was redefining the SSES SDs to reflect more realistically the dependence of the retrieval errors on observational conditions. However, this paper focuses on the SSES biases and leaves the evaluation of SSES SDs for the future work.

As documented in Petrenko et al. (2014), the baseline ACSPO SSTs (BSST; T_S) are produced with the regression equations proposed by Lavanant et al. (2012):

$$\text{Day: } T_S = a_0 + a_1 T_{11} + a_2 S_\theta T_{11} + a_3 \Delta T + a_4 T_s^0 \Delta T + a_5 S_\theta \Delta T + a_6 S_\theta, \quad (1)$$

$$\text{Night: } T_S = b_0 + b_1 T_{3.7} + b_2 S_\theta T_{3.7} + b_3 \Delta T + b_4 S_\theta \Delta T + b_5 S_\theta. \quad (2)$$

Here, $T_{3.7}$, T_{11}, and T_{12} are brightness temperatures (BTs) observed at 3.7, 11, and 12 μm, respectively; $\Delta T = T_{11} - T_{12}$; $S_\theta = \sec\theta - 1$, where θ is satellite view zenith angle (VZA); T_S^0 is the "first guess" SST (°C) obtained by interpolation of gridded L4 SST to the sensor's pixels. Currently, ACSPO uses L4 SST by the Canadian Meteorological Centre (CMC) (Brasnett 2008). Both Eqs. (1) and (2) are used in ACSPO with a single set of regression coefficients, a_i, $i = 0, 1, \ldots, 6$, and b_i, $i = 0, 1, \ldots, 5$, trained on a global dataset of matchups (MDS). Customarily, SST retrieval errors are estimated with respect to in situ SSTs. For regression algorithms, such as BSST, retrieval errors are largely caused by the inaccuracy of global approximation of a highly variable inverse relationship between BTs and SST with a single regression equation, and with a single set of coefficients. These errors essentially depend on the observational conditions, characterized by such variables as VZA, total precipitable water (TPW) vapor content in the atmosphere, wind speed, proximity to clouds, etc. (e.g., Castro et al. 2008; Xu et al. 2009; Petrenko et al. 2014).

To be realistic, the SSES should account for the dependence of BSST errors on observational conditions. This may be accomplished by separate estimation of SSES for the segments of the whole SST domain, which are relatively uniform in terms of retrieval errors. The initial ACSPO SSES algorithm (Petrenko and Ignatov 2014) performed the segmentation of the SST domain in terms of VZA and TPW. This approach, however, was found inefficient because the real number of physical variables affecting the retrieval errors is not limited to these two variables. Some approaches suggested accounting for more physical variables (underscreened cloud, aerosols, wind speed, etc.; e.g., Castro et al. 2008; Xu et al. 2009; Minnett 2014; Griffin 2014). However, it remains unclear whether accounting for all physical factors essentially affecting retrieval errors is possible.

In the redesigned ACSPO SSES, a different approach is explored, in which the retrieval errors are considered as functions of regressors (i.e., terms on the right-hand side of the regression equations, excluding the offsets) rather than certain physical variables. This way, the variations in BSST can be explained with a limited number of arguments, no matter how many physical variables on which the regressors depend. The criteria for segmentation of the SST domain in the space of regressors (**R**-space) are derived from the statistical distribution of regressors within the training MDS. During the algorithm training, these criteria are used to subdivide the global MDS into subsets of matchups belonging to specific segments. This allows for calculation of each segment's SSES SDs and local regression coefficients. At the stage of the L2 production, the SSES SDs and the local coefficients are obtained from the LUT according to the regressors' values at each pixel. The local regression coefficients are used to create an auxiliary SST product—piecewise regression SST (T_{PWR}; PWR SST)—and the SSES biases are calculated as the difference between the BSST and PWR SST.

The theoretical basis for the segmentation of the SST domain in the **R**-space is provided in section 2. The implementation of the SSES algorithm in ACSPO, version 2.4, is described in section 3. The performance of the SSES bias correction is evaluated in section 4. Section 5 summarizes and concludes the paper.

2. Segmentation of the SST domain in the space of regressors

Equations (1) and (2) can be rewritten as follows:

$$T_S = \langle T_S^{is} \rangle + \mathbf{c}^T(\mathbf{R} - \langle \mathbf{R} \rangle) + \varepsilon. \quad (3)$$

Here, $\mathbf{R}$ is a vector of regressors, T_S^{is} is in situ SST, $\mathbf{c}$ is a vector of regression coefficients, $\langle * \rangle$ denotes averaging over the global training MDS, and ε is the error of regression approximation of T_S^{is}. The vector of coefficients is estimated with the least squares method (Bard 1974) assuming that ε has a Gaussian distribution with a zero mean and SD = 1:

$$\mathbf{c} = \mathbf{D}^{-1}\langle (\mathbf{R} - \langle \mathbf{R} \rangle)(T_S^{is} - \langle T_S^{is} \rangle) \rangle. \quad (4)$$

Term $\mathbf{D}$ is a covariance matrix of regressors within the MDS:

$$\mathbf{D} = \langle (\mathbf{R} - \langle \mathbf{R} \rangle)(\mathbf{R} - \langle \mathbf{R} \rangle)^T \rangle. \quad (5)$$

The covariance matrix of the estimated vector of coefficients [Eq. (4)] is $\mathbf{D}^{-1}$. It follows from Eqs. (3)–(5) that the SST estimate [Eq. (3)] is a function of a vector of regressors $\mathbf{R}$ at a given pixel and the statistics of regressors within the training MDS, $\langle \mathbf{R} \rangle$ and $\mathbf{D}$. This suggests that the error δT_S of the SST estimate [Eq. (3)] should also be a function of these statistics. Differentiating Eq. (3) in terms of $\mathbf{c}$ gives a relationship between δT_S and the uncertainty $\delta\mathbf{c}$ of the vector of coefficients:

$$\delta T_S = \delta\mathbf{c}^T(\mathbf{R} - \langle \mathbf{R} \rangle). \quad (6)$$

The variance of δT_S is estimated from Eq. (6) as follows:

$$V(\delta T_S) = \rho^2, \quad (7)$$

$$\rho = [(\mathbf{R} - \langle \mathbf{R} \rangle)^T \mathbf{D}^{-1}(\mathbf{R} - \langle \mathbf{R} \rangle)]^{0.5}. \quad (8)$$

Parameter ρ can be viewed as a distance between $\mathbf{R}$ and $\langle \mathbf{R} \rangle$ in the $\mathbf{R}$-space. In the past, a similar parameter derived from a posteriori distribution of retrieved variables was used in the retrieval algorithms based on the inversion of the radiative transfer model. Kozlov (1966) used it as a metric in the space of retrieved variables. Merchant et al. (2008) found that the errors of the optimal SST estimation increase with ρ. Equation (7) suggests that a similar dependence takes place between the variance of the SST, estimated with Eq. (3), and the ρ derived from the distribution of regressors within the MDS. Following Kozlov (1966), we refer to the ρ as the Fisher distance in the $\mathbf{R}$-space.

Equation (7) was derived under the aforementioned assumptions regarding the error ε of the baseline regression SST. In reality, the $V(\delta T_S)$ may not be equal to ρ^2, but, as shown below in section 3, it remains a quasi-monotonic function of ρ. Therefore, a segmentation of the SST domain in terms of ρ may be viewed as a proxy for segmentation in terms of $V(\delta T_S)$. Another advantage of using ρ as a segmentation parameter follows from the fact that ρ is an argument of the Gaussian approximation of the probability density function (PDF) of $\mathbf{R}$ within the training MDS. The standard expression for this PDF (Bury 1975) has the following form:

$$P(\mathbf{R}) = [(2\pi)^N \det(\mathbf{D})]^{-0.5} \exp[-[(\mathbf{R} - \langle \mathbf{R} \rangle)^T \mathbf{D}^{-1}(\mathbf{R} - \langle \mathbf{R} \rangle)]/2]. \quad (9)$$

Considering Eq. (8), Eq. (9) can be rewritten as follows:

$$P(\mathbf{R}) = [(2\pi)^N \det(\mathbf{D})]^{-0.5} \exp[-\rho^2/2]. \quad (10)$$

Here, N is the dimensionality of $\mathbf{R}$, that is, the number of regressors from which the $\mathbf{R}$-space is constructed. It follows from Eq. (10) that ρ characterizes the extent, to which $\mathbf{R}$ is represented in the training MDS. Given the PDF by Eq. (10), ρ^2 has a χ^2 − distribution with N degrees of freedom (Bury 1975). The PDF of the χ^2 − distribution has a maximum at some small value of ρ and rapidly declines with increasing or decreasing ρ. This simplifies the segmentation process by limiting the range of considered ρ values.

Note that whereas Eq. (7) characterizes the average dependence of $V(\delta T_S)$ on ρ over all directions in the $\mathbf{R}$-space, such dependencies may vary with specific directions. For example, assuming that the mean vector $\langle \mathbf{R} \rangle$ corresponds to some "mean" value of the atmospheric absorption τ, the nonlinear dependencies of BTs on the τ may result in different dependencies of $V(\delta T_S)$ on ρ along the opposite directions corresponding to decreasing and increasing τ. To account for the anisotropy of the retrieval errors in the $\mathbf{R}$-space, we introduce an orthogonal basis consisting of N eigenvectors of the covariance matrix $\mathbf{D}$ with the origin at $\langle \mathbf{R} \rangle$ and perform segmentation in terms of ρ separately in each of 2^N orthants of this basis.

3. Implementation of SSES in ACSPO

The segmentation concept described in section 2 is the foundation of the redesigned ACSPO SSES algorithm. For the daytime, the $\mathbf{R}$-space is constructed from the

TABLE 1. Total numbers of matchups in the global MDS collected from 15 May 2013 to 8 Aug 2014, total numbers of populated segments including more than 10 matchups, and the percentages of matchups belonging to the unpopulated segments including 10 or less matchups.

Day/night	*Suomi-NPP* VIIRS	*Aqua* MODIS	*Terra* MODIS	*MetOp-A* AVHRR	*MetOp-B* AVHRR	*NOAA-19* AVHRR
Total number of matchups in the MDS						
Day	108 355	85 534	85 065	104 047	107 440	92 823
Night	113 796	85 574	89 757	120 068	116 549	94 284
Total number of segments with more than 10 matchups						
Day	202	201	199	202	206	204
Night	789	764	760	796	850	830
Percentage (%) of matchups belonging to the segments with no more than 10 matchups						
Day	0.22	0.28	0.24	0.25	0.23	0.32
Night	2.65	3.52	3.12	2.56	2.67	3.37

regressors of Eq. (1); that is, the vector of regressors has the following six components:

$$\mathbf{R} = [T_{11}, S_\theta T_{11}, \Delta T_{11-12}, T_s^0 \Delta T_{11-12}, S_\theta \Delta T_{11-12}, S_\theta]^{\mathrm{T}}. \tag{11}$$

For the nighttime, however, it was found that the five regressors appearing in Eq. (2) are not sufficient to adequately capture the full range of observational conditions. Therefore, the set of **R** components was extended and now includes the following nine components:

$$\mathbf{R} = [T_{3.7}, S_\theta T_{3.7}, \Delta T_{11-12}, \Delta T_{3.7-12}, T_s^0 \Delta T_{11-12}, T_s^0 \Delta T_{3.7-12}, S_\theta \Delta T_{11-12}, S_\theta \Delta T_{3.7-12}, S_\theta]^{\mathrm{T}}. \tag{12}$$

Here, $\Delta T_{3.7-12} = T_{3.7} - T_{12}$.

The performance of the described SSES algorithm is explored in this paper using data from six satellite sensors: *Suomi-NPP* VIIRS, *Aqua* and *Terra* MODISs, *MetOp-A* and *MetOp-B* AVHRRs [both in the full resolution area coverage (FRAC) mode with 1-km spatial resolution at nadir], and *NOAA-19* AVHRR [in the global area coverage (GAC) mode with 4-km spatial resolution at nadir], routinely processed at NOAA with ACSPO. For all these sensors, the global MDS were collected from 15 May 2013 to 8 August 2014 using clear-sky BTs selected with the ACSPO clear-sky mask (Petrenko et al. 2010) and drifting and tropical moored buoys from the NOAA in situ Quality Monitor (*i*Quam; Xu and Ignatov 2014; http://www.star.nesdis.noaa.gov/sod/sst/iquam/data.html). The in situ SSTs were selected using the *i*Quam flag showing the suitability for high-accuracy applications. Every in situ SST was matched with the nearest clear-sky satellite pixel within the 10-km distance and the time period of ±2 h.

The MDS were used to calculate the statistics $\langle \mathbf{R} \rangle$ and **D** both for day and night.

Table 1 shows the total numbers of matchups in the global MDSs for six satellite instruments mentioned above. The basis in the **R**-space with the origin at $\langle \mathbf{R} \rangle$ was introduced as a set of eigenvectors of the covariance matrix **D**, and the Fisher distances were calculated for all matchups according to Eq. (8). Figure 1 shows histograms of the matchups as functions of the Fisher distance for six sensors. Recall that the Fisher distance characterizes the extent, to which a given vector of regressors **R** is typical within a given MDS, and, at the same time, represents $V(\delta T_S)$. The shape of the histograms is similar for all sensors: the majority of matchups are concentrated within a limited range of ρ values, approximately from 1 to 6; the histograms have maximums near $\rho \approx 2$ and sharply decline with decreasing and increasing ρ. Figures 2 and 3 show daytime and nighttime global biases and SDs of the BSST and PWR SST, as functions of ρ, respectively. The statistics are relatively stable in the range $1 < \rho < 6$, and less so outside this interval, due to decreasing density of matchups (cf. Fig. 1). Note that ρ is not necessarily equal to $V(\delta T_S)^{0.5}$, as predicted by Eq. (7) for an ideal case of standard Gaussian error of the regression SST. However, the SDs in Figs. 2 and 3 near-monotonically increase with ρ within the interval of stability, for all sensors and for both BSST and PWR SST, during both day and night, adding confidence in the selection of ρ as the characteristic variable of the SSES parameterization. Note also that compared with the BSSTs, the PWR SSTs consistently produce more uniform biases and smaller SDs, which are additionally more consistent between different sensors.

The segmentation of the SST domain is performed by partitioning each orthant of the **R**-space into 10 bins with values of Fisher distance falling into the intervals $j - 1 < \rho < j$, $j = 1, 2, \ldots, 10$. Given N is the

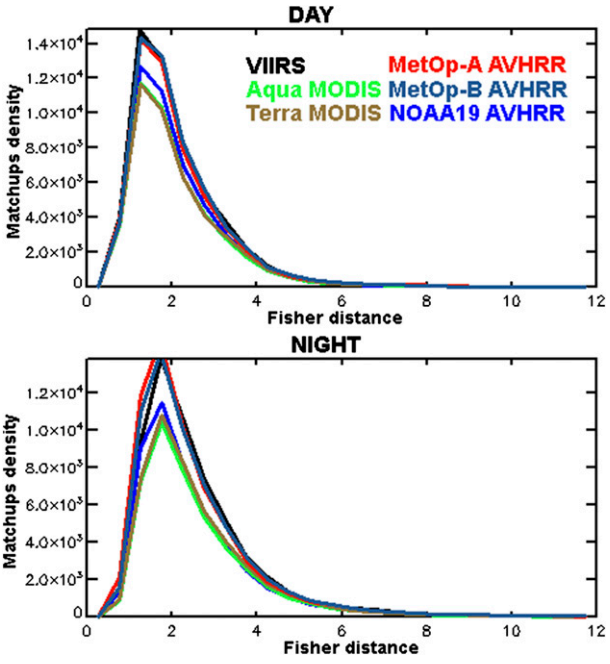

FIG. 1. Histograms of Fisher distance produced from (top) daytime and (bottom) nighttime matchups within the global MDS collected from 15 May 2013 to 8 Aug 2014 (bin size $\Delta\rho = 1.0$).

dimensionality of **R**, the total number of segments is 10×2^N, which corresponds to 640 segments for the daytime and 5120 segments for the nighttime algorithms. The number of matchups in these subsets is quite nonuniform, ranging from 0 to several thousands. SSES SDs and local regression coefficients are only calculated for "populated" segments that include more than 10 matchups. Table 1 also shows the total numbers of populated segments and the percentages of matchups belonging to the "unpopulated" segments with 10 matchups or fewer. The number of populated segments in all cases is much less than the total numbers of considered segments. The fraction of matchups falling into the unpopulated segments is 0.2%–0.3% for day and reaches 2%–3% for night, due to more detailed segmentation of the nighttime **R**-space. For the unpopulated segments, SSES biases are set to 0 and SSES SDs are filled with not-a-number (NaN) value, indicating that the corresponding SSES estimates are unavailable.

When processing satellite data, the local regression coefficients are used to calculate the PWR SST. Special measures are taken to avoid amplification of PWR SST errors caused by calculation of coefficients from a small subset of matchups. Vectors **f** of local regression coefficients are calculated as follows:

$$\mathbf{f} = \mathbf{E}^{-1}\langle\langle(\mathbf{X} - \langle\langle\mathbf{X}\rangle\rangle)(T_{\text{in situ}} - \langle\langle T_{\text{in situ}}\rangle\rangle)\rangle\rangle. \quad (13)$$

Here, $\langle\langle * \rangle\rangle$ denotes averaging over a given subset of matchups and **E** is a matrix constructed from the local covariance matrix of regressors **F** by omitting the eigenvectors corresponding to the eigenvalues smaller than $k\lambda_{\max}$ (where $\lambda_{\max}$ is the maximum eigenvalue of **F**). The value of the multiplier $k = 10^{-8}$ has been chosen empirically to provide a reasonable trade-off between the accuracy of fitting in situ SST with PWR SST and the amplification of random noise in PWR SST. As a result, the number of degrees of freedom for the estimated vector of coefficients is usually less than the number of regressors N.

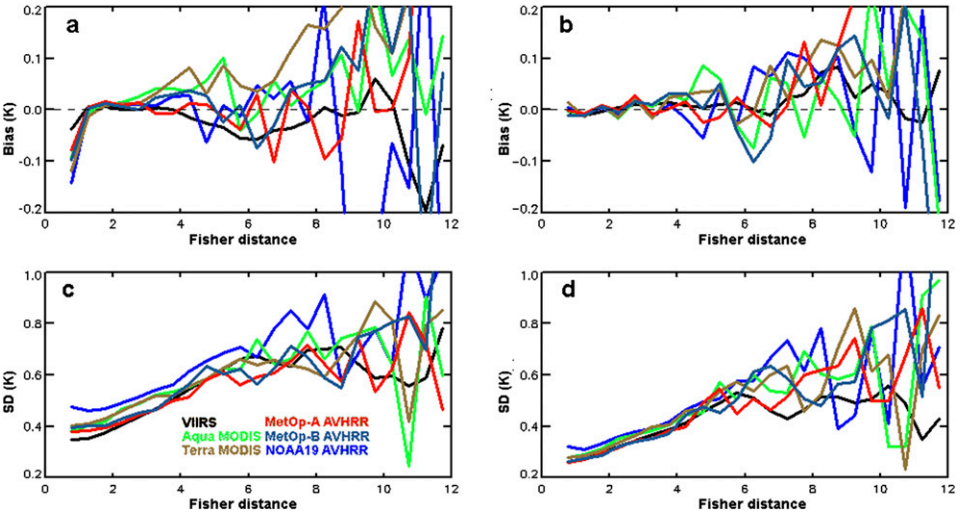

FIG. 2. Daytime (a),(b) biases and (c),(d) SDs of (a),(c) BSST and (b),(d) PWR SSTs w.r.t. in situ SST as functions of Fisher distance. Data from the same MDS as in Fig. 1.

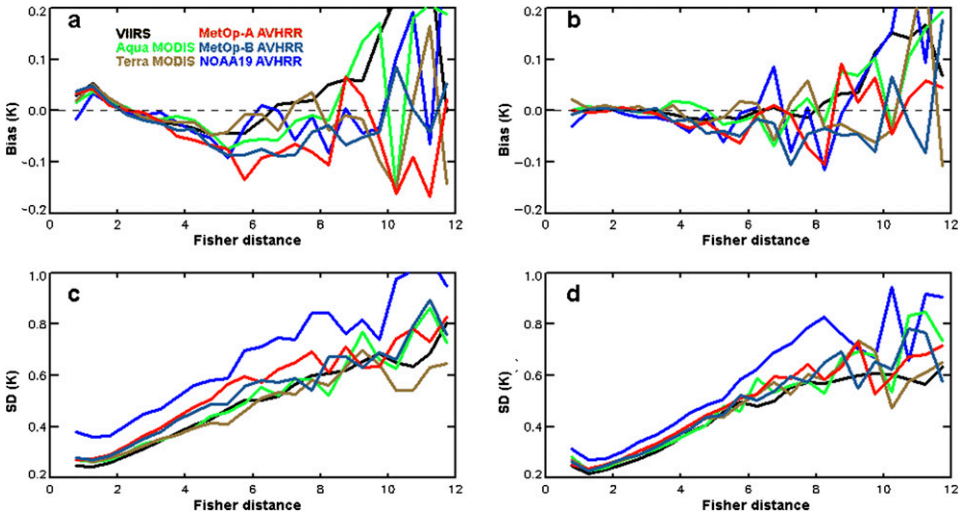

FIG. 3. As in Fig. 2, but for nighttime data.

The local regression coefficients and SSES SDs for all segments are stored in the LUT along with other data required for calculation of ρ and attributing pixels to the specific orthants in the **R**-space: $\langle \mathbf{R} \rangle$, eigenvalues, and eigenvectors of **D**. In ACSPO operational processing, each pixel is first ascribed to a specific segment. If the SSES SD for this segment is not NaN, then the following procedures are performed for this pixel: 1) PWR SST is calculated using the local regression coefficients; 2) SSES bias is calculated as BSST minus PWR SST; and 3) SSES SD is set to the corresponding LUT value. Otherwise, if the LUT value of SSES SD is NaN, then SSES bias is set to 0 and SSES SD is set to NaN for this pixel. We expect that this algorithm will be further optimized in the future versions of ACSPO.

4. The performance of SSES bias correction

As stated in section 3, the SSES bias is defined as the difference between the BSST and the PWR SST. Applying the SSES biases to the BSST transforms it back into the PWR SST. Hence, the PWR SST is an equivalent of the debiased BSST. In this section, we evaluate the performance of the SSES bias correction by comparing the statistics of BSST and PWR SST with respect to in situ SST and illustrate it with results of processing satellite data with the ACSPO, version 2.40.

TABLE 2. The ECT, global biases, and SDs of fitting in situ SST with BSST, PWR SST, and CMC SST over the full MDS collected from 15 May 2013 to 8 Aug 2014, for six sensors.

SST product	Statistics (K)	*Suomi-NPP* VIIRS	*Aqua* MODIS	*NOAA-19* AVHRR	*Terra* MODIS	*MetOp-A* AVHRR	*MetOp-B* AVHRR
ECT		1330	1330	1330	1030	0930	0930
Day							
BSST	Bias	0	0	0	0	0	0
	SD	0.41	0.45	0.50	0.46	0.43	0.44
PWR SST	Bias	0	0	0	0	0	0
	SD	0.31	0.33	0.34	0.32	0.31	0.30
CMC SST	Bias	−0.19	−0.20	−0.21	−0.06	−0.01	−0.01
	SD	0.34	0.34	0.35	0.31	0.30	0.30
Night							
BSST	Bias	0	0	0	0	0	0
	SD	0.33	0.35	0.46	0.35	0.38	0.36
PWR SST	Bias	0	0	0	0	0	0
	SD	0.25	0.26	0.29	0.26	0.27	0.26
CMC SST	Bias	0.01	0.02	0.02	−0.04	−0.07	−0.07
	SD	0.27	0.28	0.29	0.29	0.31	0.29

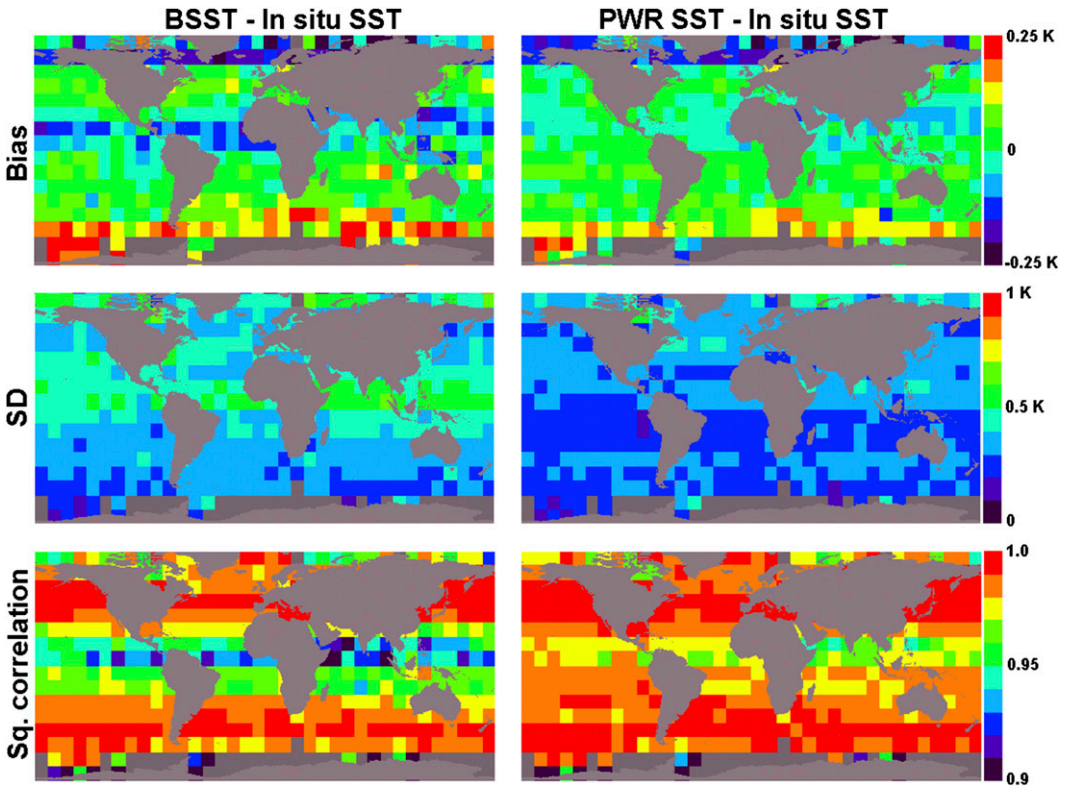

FIG. 4. Daytime statistics of (left) BSST and (right) PWR SSTs w.r.t. in situ SST, stratified within 10° lat × 10° lon boxes: (top) biases, (middle) SDs, and (bottom) squared correlation coefficients.

Table 2 compares the global statistics of fitting in situ SST with the BSST and PWR SSTs over the full global MDS collected for six satellite sensors from 15 May 2013 to 8 August 2014, as described in section 3. Table 2 also shows the equator crossing times (ECT) for these sensors. Since, in this case, the same MDS were used for both training and validation, the global biases for both algorithms are 0. The PWR SST fits the in situ SST substantially more precisely than the BSST: the corresponding SDs are reduced from 0.41–0.50 to 0.31–0.34 K for the daytime, and from 0.33–0.46 to 0.25–0.30 K for the nighttime. Table 2 also shows the statistics of fitting the same in situ SSTs with the CMC SST, interpolated to satellite pixels. Recall that the CMC is a foundation SST produced mainly from the nighttime data. Therefore, it is very consistent with the nighttime satellite data (although slightly biased cold with respect to the nighttime matchups for the morning platforms *Terra*, *MetOp-A*, and *MetOp-B*) but significantly biased cold with respect to daytime matchups for the afternoon platforms *Suomi-NPP*, *Aqua*, and *NOAA-19*. The PWR SSTs make the global SDs with respect to matchups comparable to (or even smaller than) the corresponding SDs for CMC but does not produce global biases typical for CMC.

In addition to the metrics commonly used to evaluate the performance of the SST algorithms, bias, and SD with respect to in situ SST, Merchant et al. (2009) introduced another informative metric—sensitivity of retrieved SST to variations in true SST. This analytical metric is calculated by replacing observed BTs in the regression equation with simulated derivatives of the BTs in terms of SST, and setting the corresponding offset to 0. This metric, however, is not fully applicable to the PWR SST. The input for existing radiative transfer models, such as the Community Radiative Transfer Model (CRTM; available online at http://ftp.emc.ncep.noaa.gov/jcsda/CRTM/) is "skin" SST, that is, the temperature of the upper ~10-μm layer of the ocean rather than depth SST measured by drifting and moored buoys (Donlon et al. 2007). Therefore, the theoretically estimated sensitivity characterizes the response of satellite SST retrievals to skin rather than depth SST. On the other hand, the fact that the PWR SST precisely fits in situ SST suggests that it may be viewed as an estimate of depth SST. In this study, we evaluate the responses of BSST and PWR SST to variations in depth (rather than skin) SST, using a squared correlation coefficient η^2 between the satellite and in situ SSTs. The meaning of η^2 may be explained with

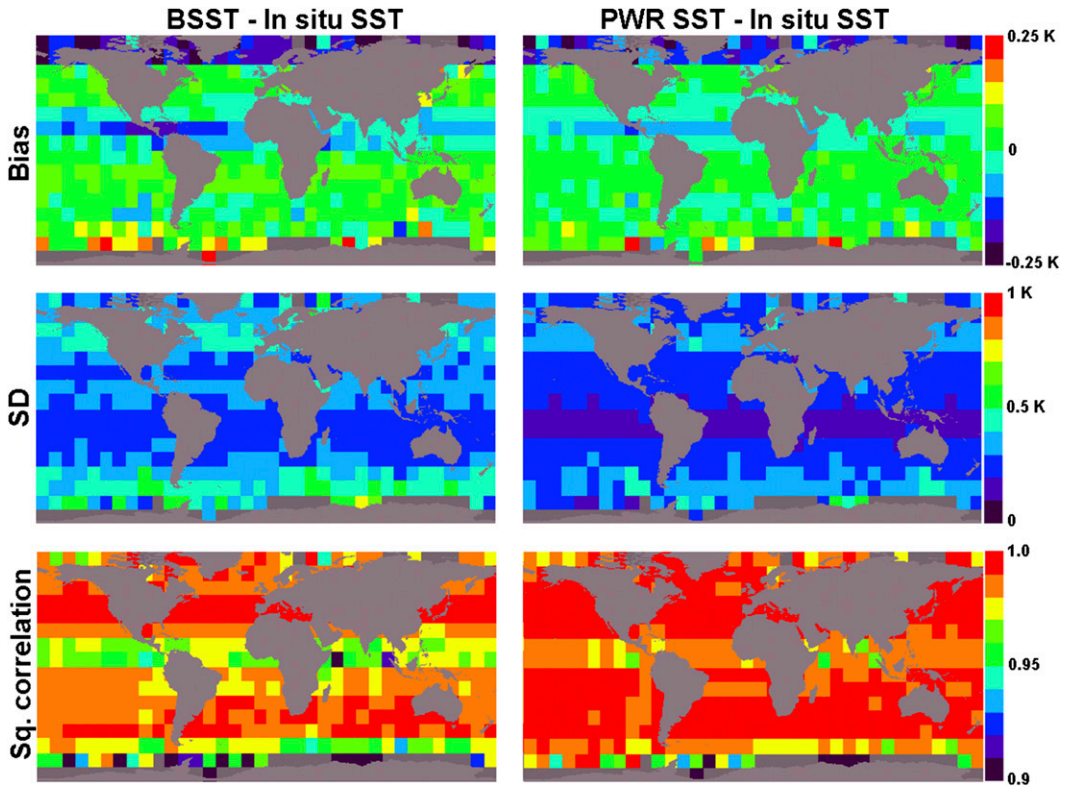

FIG. 5. As in Fig. 4, but for nighttime.

the following relationship between the full variance of T_S, $V_0(T_S)$, and the residual variance of the regression between satellite and in situ SST, $V(T_S)$ (Bard 1974):

$$V(T_S) = V_0(T_S)(1 - \eta^2). \tag{14}$$

As follows from Eq. (14), η^2characterizes a part of the $V_0(T_S)$ explained by variations in in situ SST.

Figures 4 and 5 show geographical distributions of the biases, SDs, and squared correlations for VIIRS BSST and PWR SST produced from the global MDS by aggregating matchups within 10° latitude × 10° longitude boxes. Daytime BSST biases in Fig. 4 are mostly within 0–0.1 K in the midlatitudes but significantly positive in the Southern Hemisphere high latitudes and negative in the tropics (between 0° and 20°N) and to the north of 60°N. The PWR SST reduces the negative biases in the low latitudes, and to a lesser degree the positive biases in the Southern Hemisphere high latitudes. The biases in the northern and southern high latitudes, however, remain significant. This will be a subject of future work. The reduction in daytime SDs from BSST to PWR SSTs is 0.1–0.2 K over the most part of the global ocean. The squared correlation between the BSST and in situ SST has a minimum in the tropics, likely due to the effects of daytime surface warming and large atmospheric humidity, which significantly reduces the effect of SST at the top of atmosphere. The PWR SST is better than BSST correlated with buoys in the low latitudes. The nighttime regional statistics shown in Fig. 5 demonstrate similar features, but with a lesser difference between BSST and PWR SST, because the nighttime SST algorithm uses a much more transparent band centered at 3.7 μm and because of the absence of the effect of the daytime surface warming.

The described SSES methodology was implemented in ACSPO, version 2.40, and used in L2 processing of satellite data. According to the methodology described in

TABLE 3. The fractions (%) of clear-sky pixels in which SSES SD is not defined, for six sensors (31 Jan 2015).

Day/night	*Suomi-NPP* VIIRS	*Aqua* MODIS	*Terra* MODIS	*MetOp-A* AVHRR	*MetOp-B* AVHRR	*NOAA-19* AVHRR
Day	0.52	0.37	0.22	0.41	0.32	0.63
Night	2.07	2.34	2.14	2.25	2.52	2.66

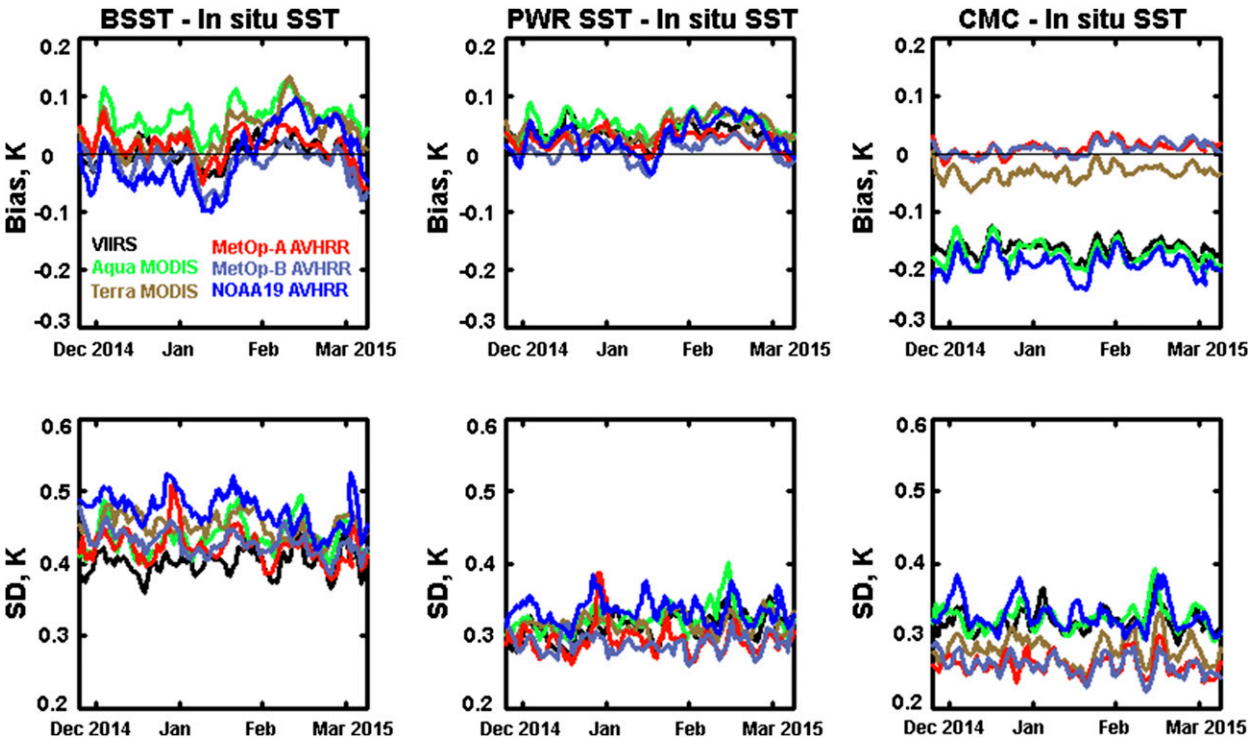

FIG. 6. Time series of daily daytime global biases and SDs of fitting in situ SST with BSST, PWR SST, and CMC, for six satellite sensors, from 24 Nov 2014 to 10 Mar 2015.

section 3, the SSES are defined during training for those pixels that belong to the populated segments represented in the training MDS with more than 10 matchups. This has allowed providing the SSES estimates for the overwhelming part of the clear-sky ocean pixels. As an example, the relative fractions of the clear-sky SST pixels with undefined SSES are shown in Table 3 from one day (31 January 2015) of observations with six sensors. The numbers in Table 3 are very consistent with the fractions of matchups falling in the unpopulated segments shown in Table 1.

Figures 6 and 7 show results of validation of BSST and PWR SST using the independent datasets of matchups. Figure 6 shows time series of daytime biases and SDs for the BSST, PWR SST, and CMC SST with respect to in situ SST for six sensors from 24 November 2014 to 10 March 2015. All curves were smoothed with a 7-day running window. To discern the difference in the effects of the diurnal surface warming on the sensors with different ECT, only those matchups were used for which the time difference between satellite and in situ SST measurements did not exceed 1 h. The daytime statistics for PWR SST in Fig. 6 are more stable and consistent between the sensors than the statistics for BSST. The peak-to-peak ranges for the global SDs are reduced from ~0.35–0.52 K for BSST to ~0.27–0.38 K for PWR SST. The corresponding biases in the foundation CMC SST are close to zero for the midmorning *MetOp-A* and *MetOp-B* satellites, slightly negative for the late-morning *Terra*, and close to −0.2 K for the afternoon *Suomi-NPP*, *Aqua*, and *NOAA-19*. The PWR SST brings global daytime SDs close to the CMC, but unlike CMC it produces small and more consistent biases for all platforms. This suggests that daytime ACSPO SSTs corrected for SSES bias can be now assimilated into the L4 analyses, on equal footing with the nighttime data (recall that current L4s exclude daytime data with low winds from analyses) and even used to produce a daytime foundation L4 SST product, with performance comparable with the existing L4 SSTs produced from nighttime SST retrievals.

Figure 7 shows similar time series for night. As in Fig. 6, the PWR SST reduces global biases and SDs compared with the BSST and improves cross-platform consistency of the statistics. The nighttime CMC biases are more consistent between the sensors than during daytime, although the biases for the midmorning platforms *MetOp-A*, *MetOp-B*, and *Terra* are now colder than for the afternoon platforms *Suomi-NPP*, *Aqua*, and *NOAA-19*. As for the daytime, both the nighttime global SDs of PWR SST and CMC SST are much lower than for the BSST.

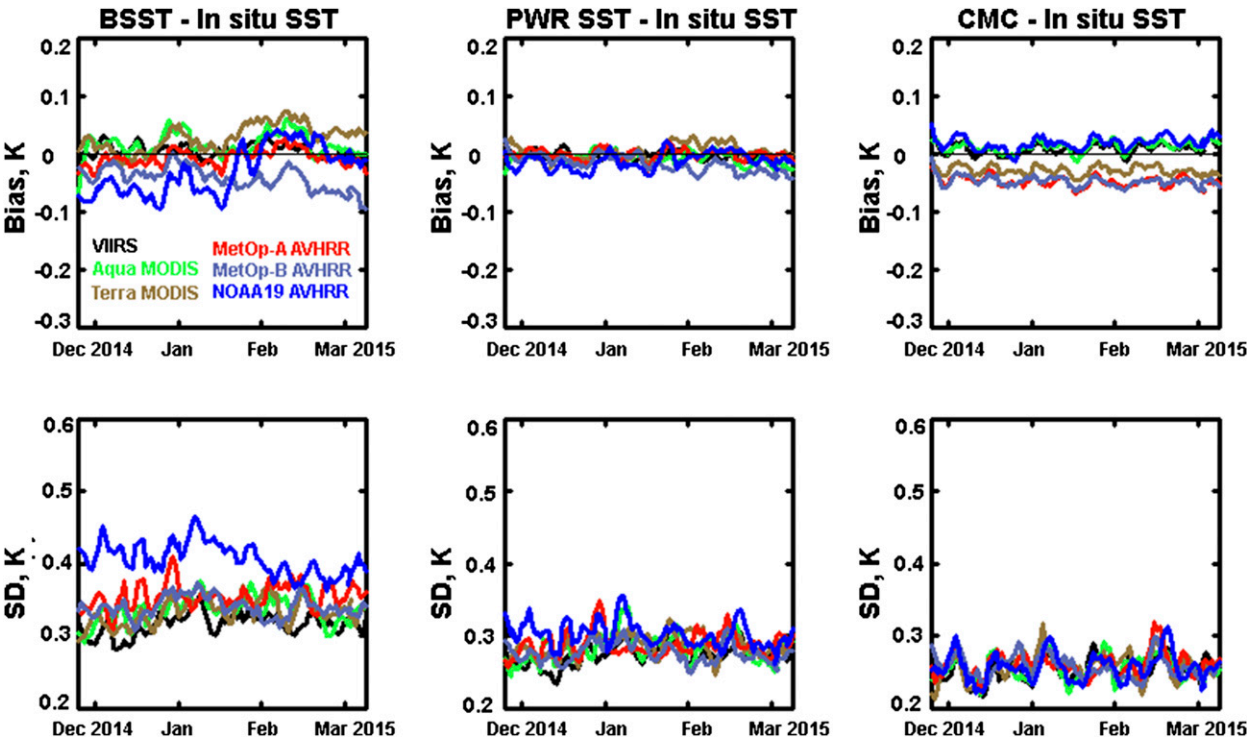

FIG. 7. As in Fig. 4, but for nighttime.

It is important to note that the correction of SSES biases in the ACSPO, version 2.40, provides the reduction of instantaneous biases in every given SST image. Figure 8 demonstrates the effect of the daytime bias correction by comparing the images of BSST minus CMC, SSES bias, and PWR SST minus CMC in a swath projection taken over the equatorial Pacific Ocean on 19 December 2014. Cloud leakages in BSST are seen in the left image as a fringe of colder pixels surrounding clouds, whereas areas with warm deviations of BSST from CMC SST are due to diurnal surface warming. The image in the middle demonstrates that the SSES bias effectively captures both effects. As a result, the biases are reduced in the right image, showing the deviations of PWR SST from CMC.

Figure 9 shows an example of nighttime imagery in the swath projection. The left image shows typical angular artifacts in BSST minus CMC. The BSST is slightly colder than CMC SSTs in the middle and at the edges of the swath, and slightly warmer at intermediate VZAs. Cold biases caused by cloud leakages are also present. The SSES bias shown in the middle image effectively accounts for both artifacts in the BSST, which makes the deviations of the PWR SST from CMC more flat and uniform.

Figure 10 demonstrates the effects of SSES bias correction on the deviations of ACSPO SST from CMC SST for *Suomi-NPP* VIIRS observations on 16 February 2015. The deviations of BSST from CMC are mainly caused by cloud leakages and by variations in VZA. During the daytime, warming in the upper surface layer of the ocean is another factor. SSES biases capture all these effects, to a different degree. The SSES bias correction appears efficient, as evidenced by noticeably more uniform images of the PWR SST − CMC SST compared with the BSST − CMC SST. Note that Fig. 10 represents a stringent test in the full VIIRS retrieval domain for the SSES that was developed from matchups with in situ data that are available only in its constrained subspace.

5. Summary and conclusions

The redesigned ACSPO SSES algorithm defines bias of the baseline SST product [BSST, estimated with Eqs. (1) and (2)] as the difference between the BSST and the piecewise regression SST (PWR SST) introduced in this study. Applying SSES biases to the BSST transforms it back into the PWR SST. Comparison of the performance of the BSST and PWR SST shows that the SSES bias correction substantially improves a global agreement with in situ SST. This is achieved by 1) segmentation of the SST retrieval domain in the space of regressors (rather than in the space of physical variables

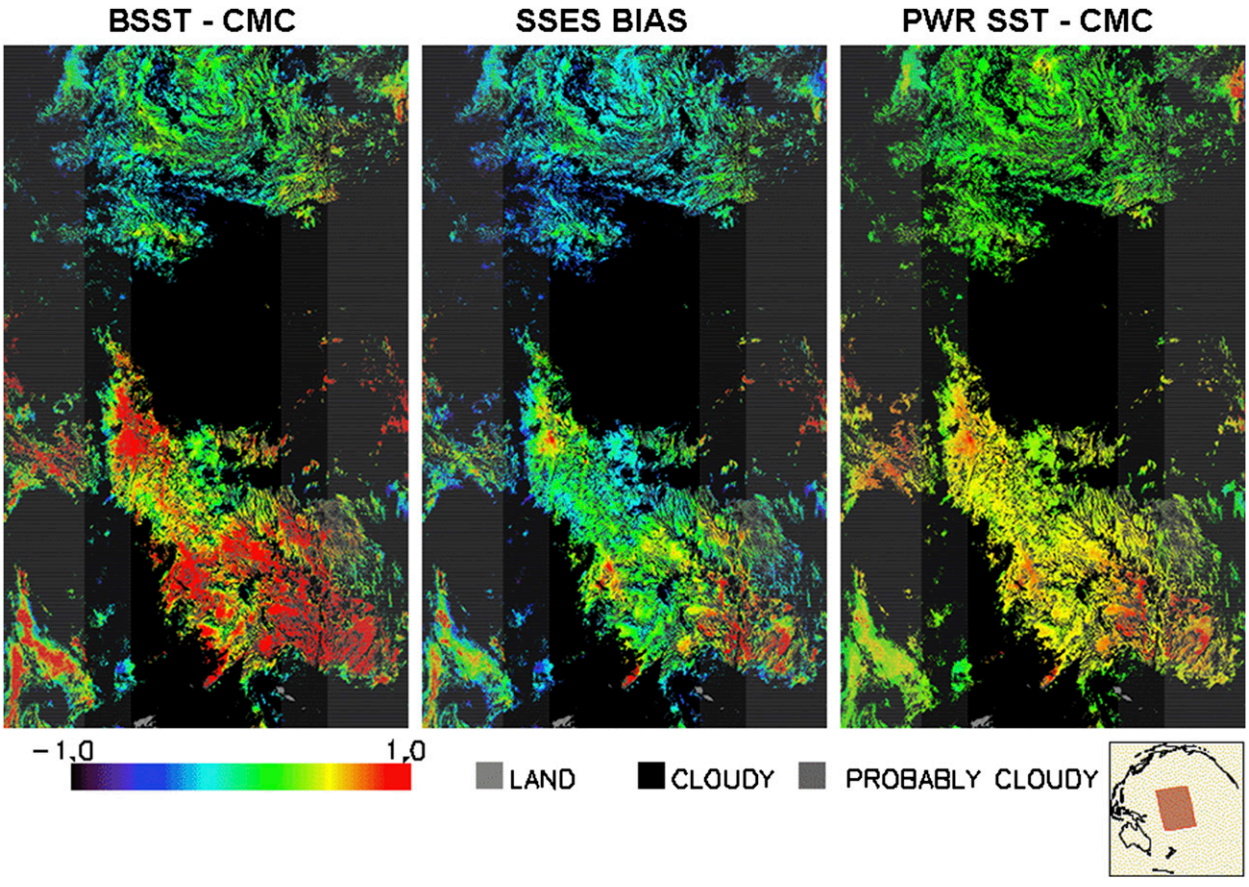

FIG. 8. Daytime images of BSST − CMC SST, PWR SST − CMC SST, and SSES bias in swath projection from *Suomi-NPP* VIIRS on 19 Dec 2014 over the equatorial Pacific Ocean.

as is the customary practice in the SST community); 2) deriving the segmentation criteria from the statistical structure of regressors within the training MDS; and 3) defining the debiased BSST as PWR SST calculated with local regression coefficients, separately derived for each segment.

The performance of the ACSPO PWR SST gives a new perspective to the question, To what extent the precision of fitting in situ SST with global regression SST algorithm can be improved by stratification of regression coefficients? The piecewise regression methodology was previously implemented in Pathfinder AVHRR and NASA MODIS SST processing (Evans and Podesta 1998; Kilpatrick et al. 2001, 2015; Casey et al. 2010) and in the more recent latitude band (LATBAND; Minnett and Evans 2009) algorithms. In the current Pathfinder AVHRR SST product, regression coefficients are stratified in terms of BT difference between 11- and 12-μm bands, considered a proxy for the atmospheric humidity. LATBAND introduces separate sets of coefficients for each 20° latitudinal band. Both of these algorithms have reduced global SD with respect to in situ SST by ~0.02 K compared to the case of using the same equation with a single global set of coefficients (Table 2 in Petrenko et al. 2014). In the redesigned ACSPO SSES algorithm, the PWR SST reduces global SD by 0.10–0.15 K during the day and by 0.08–0.15 K at night, bringing the global SDs in the satellite-retrieved PWR SST to the level typical for ''foundation'' L4 SST products, such as the CMC or Operational Sea Surface Temperature and Sea Ice Analysis (OSTIA; Donlon et al. 2012).

Thus, the ACSPO, version 2.40, effectively provides users with two SST products, the BSST and the PWR SST. The PWR SST is not reported in the output ACSPO files as a separate layer, but it can be easily obtained by subtracting the SSES bias from the BSST. These two products have different characteristics. The BSST provides a reasonable combination of precision with respect to in situ SST and sensitivity to ''skin'' SST (Petrenko et al. 2014). The PWR SST correlates and agrees with in situ SST much better than does the BSST, but it does not guarantee high sensitivity to skin SST. Therefore, the PWR SST can be viewed as an estimate of depth SST.

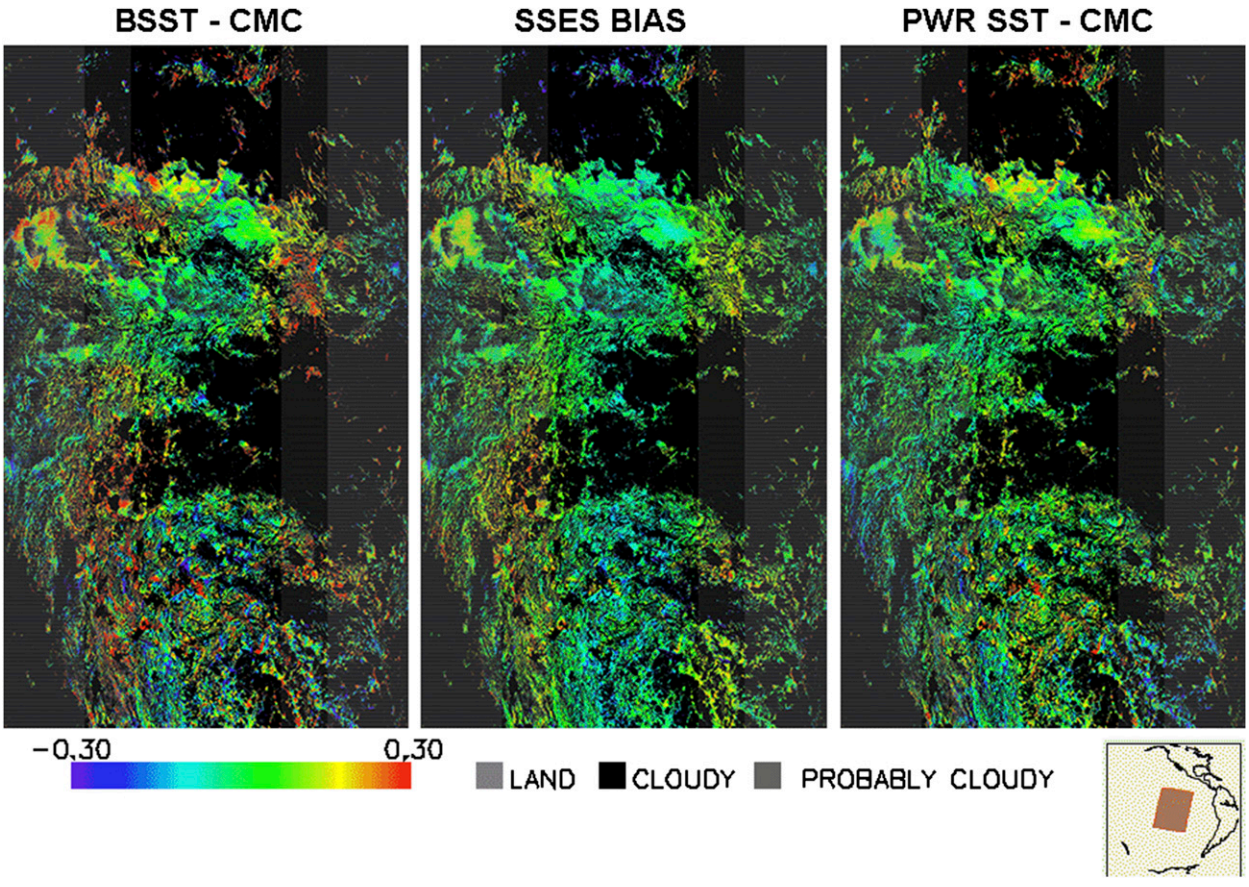

FIG. 9. Nighttime images of BSST − CMC SST, SSES bias, and PWR SST − CMC SST in swath projection produced from *Suomi-NPP* VIIRS observations on 19 Dec 2014 over the equatorial Pacific Ocean.

A full range of potential applications of the PWR SST has yet to be determined. In particular, it is expected to benefit producers of the foundation (CMC, OSTIA) and depth (Reynolds) L4 SSTs, by reducing or eliminating the need in the L4-specific "bias correction" during assimilation of ACSPO SST data. The fact that the global precision of daytime PWR SST is now comparable with the precision of L4 SST (with the additional bonus of not showing sensor-dependent biases with respect to matchups) suggests that daytime ACSPO SST can be now successfully assimilated into the L4 SST, similarly to the nighttime retrievals, or they can be used to create a daytime L4 SST from the daytime PWR SST. We emphasize, however, that although all analyses in this study consistently suggest that the new ACSPO SSES should be of interest to L4 producers and have a positive effect on their analyses, the ultimate test is assimilation into L4. Work is currently underway with different L4 groups, and its results will be reported elsewhere.

Along with SSES bias, which was discussed in this study in detail, the ACSPO, version 240, also reports SSES SD estimated as SD of BSST minus in situ SST for specific segments. The performance of the SSES SD has yet to be evaluated. This can be done, for example, by using it to better define the optimal weights with which BSST should be assimilated into the L4 SST product. Note that the SSES SD for the PWR SST has not been included in the ACSPO, version 2.40, output because the GDS 2.0 format allows for only one SSES set. However, SSES SD for the PWR SST may be easily added to the ACSPO output per users' request. The redesigned SSES algorithm presented in this paper and implemented in version 2.40 of ACSPO should not be considered a final version and will be further optimized in the future. At this point in time, the following potential areas of improvement are envisioned.

1) The fundamental limitation of the segmentation algorithm is that some of the segments are represented within the training MDS with insufficient numbers of matchups. This makes the SSES estimates for such segments less reliable. The current SSES LUTs have been derived from MDS covering more than a year-long time period, from 15 May 2013 to 8 August 2014.

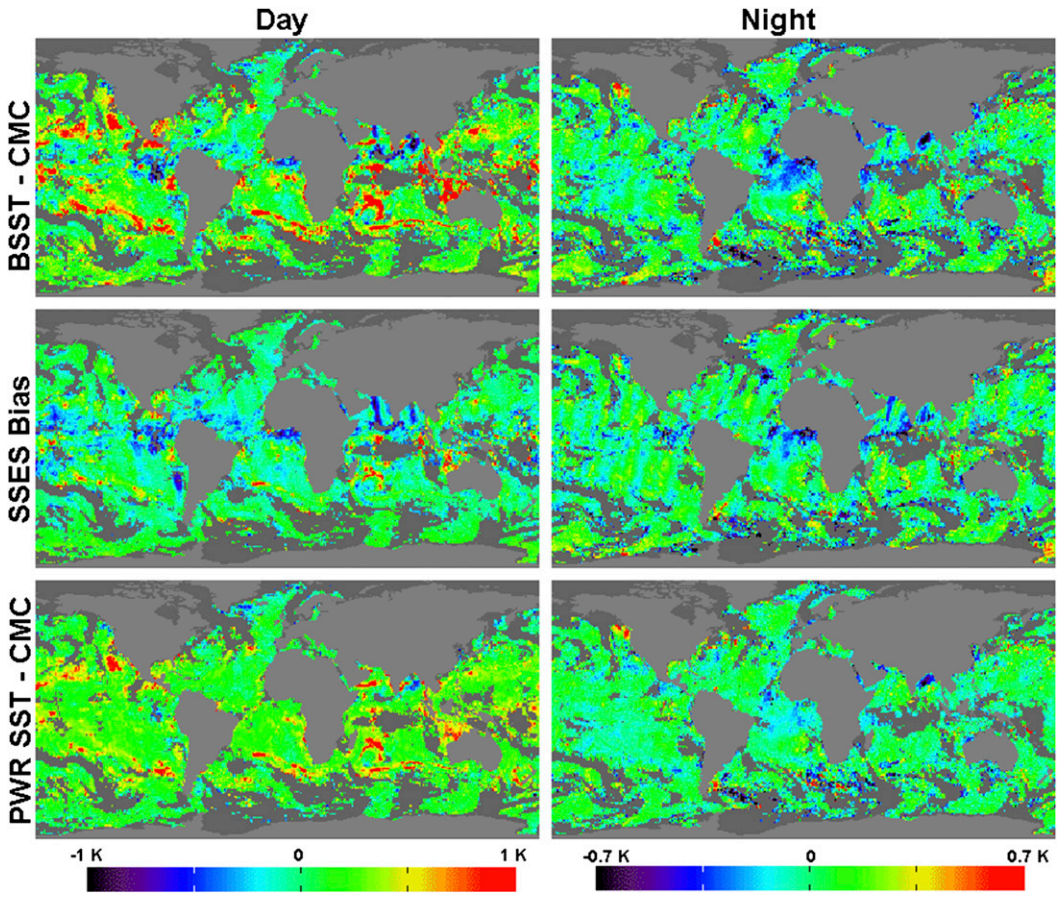

FIG. 10. (left) Daytime and (right) nighttime geographical distributions of (top) BSST − CMC SST, (middle) SSES bias, (bottom) PWR SST − CMC SST from *Suomi-NPP* VIIRS observations on 16 Feb 2015.

This time period may be further extended to ensure better coverage of the problematic segments, provided that the sensor's calibration remains stable.

2) More detailed segmentation of the SST domain might allow for better discrimination of the SSES for different observational conditions, but it would further reduce reliability of SSES estimates due to reducing the number of matchups belonging to each segment. Further optimization of the segmentation algorithm will be explored for a better trade-off between the two factors mentioned above.
3) Visual analysis of the PWR SST imagery shows that most of the images do not include discernible artifacts and discontinuities, although they are often composed from different segments with different local regression coefficients and SSTs. However, the possibility of such undesirable effects is not excluded. This problem also will be addressed in the next version of ACSPO.
4) In addition to SSES, the GDS2 format requires assessing the quality of L2 SST pixels using an incremental scale from 0 to 5, where 0 corresponds to the worst quality and 5 indicates the best-quality data. Currently, the definitions of quality levels in ACSPO are independent of SSES and based on the ACSPO clear-sky mask (Petrenko et al. 2010): levels 5 and 4 correspond to "clear" and "probably clear" pixels, respectively, and level 0 is assigned to all other pixels. In section 2 we introduced an additional metric for the quality of the SST estimate—Fisher distance, which directly links the standard deviation of a given SST estimate to the structure of the training MDS. In the future this parameter can be used for further specification of the ACSPO quality levels.

Acknowledgments. This work was conducted under the JPSS and Geostationary Operational Environmental Satellite-R Series (GOES-R) SST projects funded by the JPSS and GOES-R program offices, respectively. We thank JPSS Program Scientist Mitch Goldberg and GOES-R Manager Jaime Daniels. We also appreciate support of the NOAA Ocean Remote Sensing Program (Program Manager: Paul

DiGiacomo). Thanks also go to our NOAA colleagues John Sapper, John Stroup, Xingming Liang, Xinjia Zhou, and Feng Xu for their assistance, the discussions, and the feedback at the manuscript's different stages. The views, opinions, and findings contained in this paper are those of the authors and should not be construed as an official NOAA or U.S. government position, policy, or decision.

APPENDIX

List of Acronyms

The list of acronyms used in this paper is given below. (Additional expansions of acronyms are available online at http://www.ametsoc.org/PubsAcronymList.)

ACSPO	Advanced Clear-Sky Processor for Oceans
AVHRR	Advanced Very High Resolution Radiometer
BT	Brightness temperature
CMC	Canadian Meteorological Centre
GAC	Global area coverage mode
CRTM	Community Radiative Transfer Model
GHRSST	Group for High Resolution SST
ECT	Equator crossing time
EUMETSAT	European Organisation for the Exploitation of Meteorological Satellites
FRAC	Full resolution area coverage
GDS2	GHRSST Data Specification revision 2.0
iQuam	In situ Quality Monitor
L2	Level 2
L4	Level 4
LUT	Lookup table
MDS	Dataset of matchups
MetOp-A	*Meteorological Operational-A*
Met-Op-B	*Meteorological Operational-B*
MODIS	Moderate Resolution Imaging Spectroradiometer
NASA	National Aeronautics and Space Administration
NAVO	Naval Oceanographic Office
NOAA	National Oceanic and Atmospheric Administration
OSI SAF	Satellite Application Facility on Ocean and Sea Ice
OSTIA	Operational Sea Surface Temperature and Sea Ice Analysis
PDF	Probability density function
PWR SST	Piecewise Regression SST
Suomi-NPP VIIRS	*Suomi–National Polar-Orbiting Partnership*
R-space	Space of regressors
TPW	Total precipitable water vapor content in the atmosphere
SD	Standard deviation
SSES	Sensor-specific error statistics
SST	Sea surface temperature
VIIRS	Visible Infrared Imaging Radiometer Suite
VZA	Satellite view zenith angle

REFERENCES

Bard, Y., 1974: *Nonlinear Parameter Estimation*. Academic Press, 351 pp.

Brasnett, B., 2008: The impact of satellite retrievals in a global sea-surface-temperature analysis. *Quart. J. Roy. Meteor. Soc.*, **134**, 1745–1760, doi:10.1002/qj.319.

Bury, K. V., 1975: *Statistical Models in Applied Science*. John Wiley & Sons, 625 p.

Casey, K. S., T. B. Brandon, P. Cornillon, and R. Evans, 2010: The past, present, and future of the AVHRR Pathfinder program. *Oceanography from Space*, Springer, 273–287, doi:10.1007/978-90-481-8681-5_16.

Castro, S., G. Wick, D. Jackson, and W. Emery, 2008: Error characterization of infrared and microwave sea surface temperature products for merging and analysis. *J. Geophys. Res.*, **113**, C03010, doi:10.1029/2006JC003829.

Cayula, J. F., D. May, B. McKenzie, D. Olszewski, and K. Willis, 2004: Reliability estimates for real-time sea surface temperature. *Sea Technol.*, **45** (2), 67–73.

Donlon, C., and Coauthors, 2007: The Global Ocean Data Assimilation Experiment High-Resolution Sea Surface Temperature Pilot Project. *Bull. Amer. Meteor. Soc.*, **88**, 1197–1213, doi:10.1175/BAMS-88-8-1197.

——, M. Martin, J. Stark, J. Roberts-Jones, E. Fiedler, and W. Wimmer, 2012: The Operational Sea Surface Temperature and Sea Ice Analysis (OSTIA) system. *Remote Sens. Environ.*, **116**, 140–158, doi:10.1016/j.rse.2010.10.017.

Evans, R., and G. P. Podestá, 1998: Pathfinder sea surface temperature algorithm. [Available online at http://yyy.rsmas.miami.edu/groups/rrsl/pathfinder/Algorithm/algo_index.html.]

GHRSST, 2014: Proceedings of the GHRSST XV Science Team Meeting. GHRSST, 232 pp. [Available online at https://www.ghrsst.org/documents/q/category/ghrsst-science-team-meetings/ghrsst-xv-cape-town-south-africa/.]

Griffin, C., 2014: ABoM AVHRR SSES. Proceedings of the GHRSST XV Science Team Meeting, GHRSST, 197. [Available https://www.ghrsst.org/files/download.php?m=documents&f=140909140150-GXVProceedingsCapeTownIssue1Revision0online.pdf.]

Kilpatrick, K. A., G. P. Podestá, and R. Evans, 2001: Overview of the NOAA/NASA advanced very high resolution radiometer Pathfinder algorithm for sea surface temperature and associated matchup database. *J. Geophys. Res.*, **106**, 9179–9197, doi:10.1029/1999JC000065.

——, and Coauthors, 2015: A decade of sea surface temperature from MODIS. *Remote Sens. Environ.*, **165**, 27–41, doi:10.1016/j.rse.2015.04.023.

Kozlov, V. P., 1966: On the estimation of the vertical temperature profile from the outgoing radiation spectrum. *Izv. Acad. Sci. USSR, Atmos. Oceanic Phys.*, **2** (2), 137–148.

Lavanant, L., P. Le Borgne, and G. Legendre, 2012: SST from NPP/VIIRS: Status at OSI–SAF. Proceedings of the GHRSST XIII Science Team Meeting, GHRSST, 235. [Available online at https://www.ghrsst.org/files/download.php?m=documents&f=130722141306-GHRSSTXIIIProceedingsIssue1Rev0.pdf.]

Merchant, C. J., P. Le Borgne, A. Marsouin, and H. Roquet, 2008: Optimal estimation of sea surface temperature from split-window observations. *Remote Sens. Environ.*, **112**, 2469–2484, doi:10.1016/j.rse.2007.11.011.

——, A. R. Harris, H. Roquet, and P. Le Borgne, 2009: Retrieval characteristics of non-linear sea surface temperature from the Advanced Very High Resolution Radiometer. *Geophys. Res. Lett.*, **36**, L17604, doi:10.1029/2009GL039843.

Minnett, P. J., 2014: MODIS/VIIRS SSES hypercube. Proceedings of the GHRSST XV Science Team Meeting, GHRSST, 197. [Available online at https://www.ghrsst.org/documents/q/category/ghrsst-science-team-meetings/ghrsst-xv-cape-town-south-africa/.]

——, and R. H. Evans, 2009: MODIS sea surface temperatures. *2009 Int. Users Symp.*, Santa Rosa, CA, GHRSST. [Available online at https://www.ghrsst.org/files/download.php?m=documents&f=Session2_Minnett.ppt.]

OSI-SAF, 2009: Low Earth Orbiter sea surface temperature product user manual. Version 2.1, Météo-France, 50 pp. [Available online at http://www.osi-saf.org/biblio/docs/ss1_pum_leo_sst_2_1.pdf.]

Petrenko, B., and A. Ignatov, 2014: SSES in ACSPO. Proceedings of the GHRSST XV Science Team Meeting, GHRSST, 219–220. [Available online at https://www.ghrsst.org/files/download.php?m=documents&f=140909140150-GXVProceedingsCapeTownIssue1Revision0online.pdf.]

——, ——, Y. Kihai, and A. Heidinger, 2010: Clear-sky mask for the Advanced Clear-Sky Processor for Oceans. *J. Atmos. Oceanic Technol.*, **27**, 1609–1623, doi:10.1175/2010JTECHA1413.1.

——, ——, ——, J. Stroup, and P. Dash, 2014: Evaluation and selection of SST regression algorithms for JPSS VIIRS. *J. Geophys. Res. Atmos.*, **119**, 4580–4599, doi:10.1002/2013JD020637.

Reynolds, R. W., N. A. Rayner, T. M. Smith, D. C. Stokes, and W. Wang, 2002: An improved in situ and satellite SST analysis for climate. *J. Climate*, **15**, 1609–1625, doi:10.1175/1520-0442(2002)015<1609:AIISAS>2.0.CO;2.

Xu, F., and A. Ignatov, 2014: In situ SST Quality Monitor (*i*Quam). *J. Atmos. Oceanic Technol.*, **31**, 164–180, doi:10.1175/JTECH-D-13-00121.1.

——, ——, and X. Liang, 2009: Towards continuous error characterization of sea surface temperature in the Advanced Clear-Sky Processor for Oceans. *16th Conf. on Satellite Meteorology and Oceanography*, Phoenix, AZ, Amer. Meteor. Soc., JP1.13. [Available online at https://ams.confex.com/ams/89annual/webprogram/Paper143882.html.]